Proc. Natl. Acad. Sci. USA
Vol. 95, pp. 9518–9523, August 1998
Medical Sciences

3′-Azido-3′-deoxythymidine drug resistance mutations in HIV-1 reverse transcriptase can induce long range conformational changes

(crystal structure/ddI/AIDS)

JINGSHAN REN*, ROBERT M. ESNOUF*†‡, ANDREW L. HOPKINS*, E. YVONNE JONES*†, IAN KIRBY§, JAMES KEELING§, CARL K. ROSS§, BRENDAN A. LARDER§¶, DAVID I. STUART*†‖, AND DAVID K. STAMMERS*§‖

*Laboratory of Molecular Biophysics, Rex Richards Building, South Parks Road, University of Oxford, Oxford OX1 3QU, United Kingdom; †Oxford Centre for Molecular Sciences, New Chemistry Building, South Parks Road, University of Oxford, Oxford OX1 3QT, United Kingdom; and §Glaxo Wellcome Research & Development, Langley Court, Beckenham, Kent BR3 3BS, United Kingdom

Communicated by David Phillips, University of Oxford, United Kingdom, May 27, 1998 (received for review February 10, 1998)

ABSTRACT **HIV reverse transcriptase (RT) is one of the main targets for the action of anti-AIDS drugs. Many of these drugs [e.g., 3′-azido-3′-deoxythymidine (AZT) and 2′,3′-dideoxyinosine (ddI)] are analogues of the nucleoside substrates used by the HIV RT. One of the main problems in anti-HIV therapy is the selection of a mutant virus with reduced drug sensitivity. Drug resistance in HIV is generated for nucleoside analogue inhibitors by mutations in HIV RT. However, most of these mutations are situated some distance from the polymerase active site, giving rise to questions concerning the mechanism of resistance. To understand the possible structural bases for this, the crystal structures of AZT- and ddI-resistant RTs have been determined. For the ddI-resistant RT with a mutation at residue 74, no significant conformational changes were observed for the p66 subunit. In contrast, for the AZT-resistant RT (RTMC) bearing four mutations, two of these (at 215 and 219) give rise to a conformational change that propagates to the active site aspartate residues. Thus, these drug resistance mutations produce an effect at the RT polymerase site mediated simply by the protein. It is likely that such long-range effects could represent a common mechanism for generating drug resistance in other systems.**

Nucleoside analogue inhibitors (NIs) such as 3′-azido-3′-deoxythymidine (AZT) and 2′,3′-dideoxyinosine (ddI) are used widely in the treatment of HIV infection. They act by competing with natural substrates at the HIV reverse transcriptase (RT) polymerase active site, leading to incorporation and termination of the DNA chain. Treatment of AIDS patients with NIs selects for HIV strains containing mutations in the RT, which represents a continuing problem in combating the disease, despite the encouraging results from combination drug trials (1). Resistance to AZT is associated with a series of mutations. For instance, the mutations D67N, K70R, T215F, and K219Q give a three-fold increase in K_i for AZT-triphosphate; the resultant enzyme denoted RTMC is investigated here (2). For ddI, resistance can be conferred by a single mutation at position 74 (3). Surprisingly, most of the NI resistance mutations in RT are positioned some distance from the polymerase active site in the p66 subunit. In the three-dimensional structure of HIV-1 RT (4–7), residues 215 and 219 are ≈10Å from the conserved active site aspartate residues 110, 185, and 186 whereas residues 67, 70, and 74 are in a different domain, >20 Å away (Fig. 1). The analysis of the effects of the mutations in RTMC on AZT resistance suggests that the interactions between these mutations are complex, ranging from compensatory to synergistic, although residue 215 stands out as having a pivotal role (37). In contrast to NIs, resistance mutations associated with the nonnucleoside RT inhibitors (NNI) cluster around the NNI binding pocket and presumably cause resistance through distortion of this ligand site (6, 8, 9). In the absence of structural data for NI-resistant RTs, various mechanisms have been proposed to explain the action of such mutants. These mechanisms include a repositioning of the template strand overhang, giving feed-back to the active site (10) or a postulated allosteric nucleotide site in the p51 subunit (11). A third possibility is long range conformational changes within the protein.

On the assumption that knowledge of the structural basis of resistance could aid in the design of novel drugs and could provide a basis for rational evaluation of new combinations of RT inhibitors to combat AIDS, we have determined three related structures for both the quadruple mutant RTMC and the L74V mutant HIV-1 RTs by analyzing each in different crystal forms (Table 1). All of these structures contain the NNI 1051U91 (12) but possess no ligands at the polymerase active site. Although the x-ray data sets used for structure determination do not extend to high resolution, because the crystals tend to be small and are less well ordered than wild-type RT, by taking the various results together, we may be confident of the key structural features observed.

MATERIALS AND METHODS

Protein Isolation and Crystallization. RTMC was cloned into the expression vector pKK233–2 as described (13). Purification, cocrystallization of RT with the NNI 1051U91 (12, 14), and partial dehydration of these crystals followed our described methods (12). RT bearing the L74V mutant was provided by P. Ray (Burroughs Wellcome, Research Triangle Park, NC).

X-Ray Data Collection and Processing. Diffraction data were collected at two synchrotron sources from nine crystals. These were of cell forms C, E, and F from our related series of $P2_12_12_1$ crystal forms (12, 15, 16). The data for cell form C crystals for

Abbreviations: RT, reverse transcriptase; NI, nucleoside analogue RT inhibitor; NNI, nonnucleoside RT inhibitor; AZT, 3′-azido-3′-deoxythymidine; ddI, 2′,3′-dideoxyinosine.

Data deposition: The coordinates for the RTMC structure have been deposited in the Protein Data Bank, Biology Department, Brookhaven National Laboratory, Upton, NY 11973 (PDB ID code 1RT3).

‡Present address: Rega Institute for Medical Research, Katholieké Univesiteit. Leuven, Minderbroedersstraat 10, B-3000 Leuven, Belgium.

¶Present address: Virco United Kingdom Limited, 162A Science Park, Milton Road, Cambridge, CB4 4GH, United Kingdom.

‖To whom reprint requests should be addressed.

The publication costs of this article were defrayed in part by page charge payment. This article must therefore be hereby marked "*advertisement*" in accordance with 18 U.S.C. §1734 solely to indicate this fact.

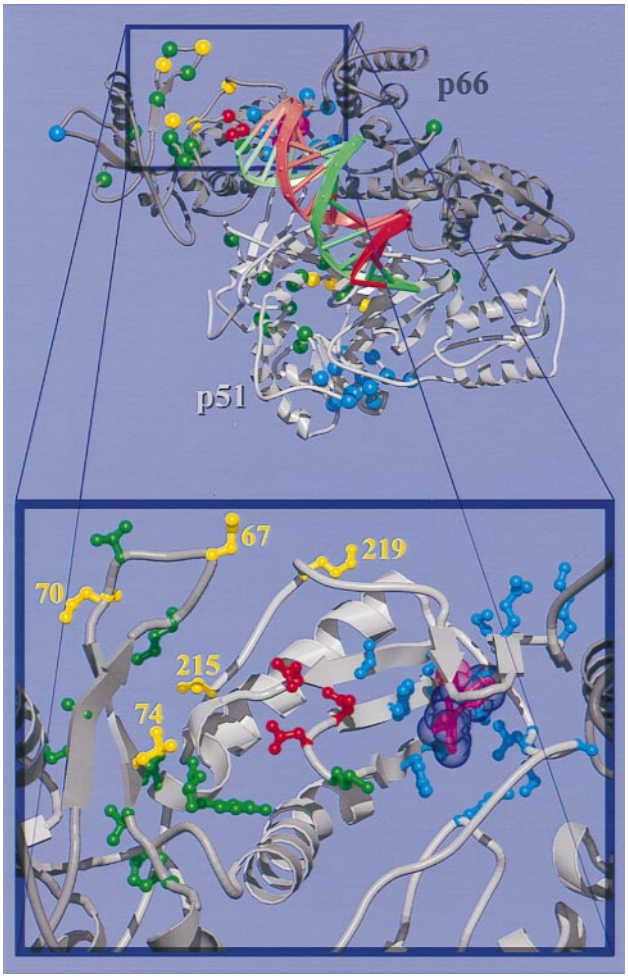

FIG. 1. Overall structure and drug resistance mutation sites of the RT heterodimer. (*Top*) The p66 subunit is drawn in dark gray and p51 in light gray. NI resistance mutation sites (26) are shown as green spheres, with RTMC and L74V sites highlighted in yellow. In the p51 subunit, residues 215 and 219 are disordered; their positions are not shown. NNI resistance mutation sites (27) are shown as blue spheres. The three polymerase active site aspartate residues and the bound NNI are shown in red and magenta, respectively. Double-stranded DNA (shown as a spiral ladder with the template strand in green and the primer in red) was modeled into our RT-nevirapine structure (6) from the Cα and phosphate coordinates of the RT-DNA-Fab complex (5) by superimposing the p66 palm domain of the two structures. (*Bottom*) A close-up view of the polymerase active site and the drug resistance mutation sites in the p66 subunit. The coloring scheme is the same as in the top panel; however, the side chains for mutated residues are shown in ball-and-stick representation and the van der Waals surface for the bound NNI (nevirapine) is shown semitransparent.

each RT mutant were merged to give single datasets, thus resulting in three datasets for each mutant of RT.

The synchrotrons used were (*i*) station BL-6A2 at the Photon Factory, National Laboratory for High Energy Physics, Tsukuba, Japan (datasets RTMC-1, RTMC-3, RTL74V-1, and RTL74V-2) using the Weissenberg method (17) following our established data collection strategy (6), except that flash-cooled crystals could not be confined within a helium-filled enclosure (*ii*) stations 9.6 [30-cm MAR-Research imaging plate (MAR-Research, Hamburg, Germany)] and 7.2 (18-cm MAR) at the Synchrotron Radiation Source, Daresbury Laboratory, Warrington, United Kingdom (datasets RTMC-2 and RTL74V-3, respectively) using 1.5° oscillations (Table 1). All crystals were flash-cooled to and maintained at 100 K except for the RTMC-3 and RTL74V-2 datasets, which were recorded at 14°C. Data processing was done with DENZO and SCALEPACK (18).

Structure Determination. The structures were solved by molecular replacement with the X-PLOR program (19) by using our best RT models for each cell form [cell form C, the RT-1051U91 complex (6); cell form E, the RT-MKC-442 complex (20); and cell form F, the RT-9-Cl-TIBO complex (16)]. A three-stage rigid-body refinement protocol was used, first as single rigid-body refinement, then as two rigid subunits (p66 and p51), and finally as nine rigid domains. Each dataset was sharpened by using anisotropic B-factor scaling as described (21).

Refinement and Electron Density Averaging. For the highest resolution dataset (RTMC-1), further careful refinement was undertaken using X-PLOR (19), namely, conjugate gradient minimization, restrained simulated annealing, strongly coupled individual atomic B factor refinement, and a bulk solvent correction. In all refinements, particular care was taken to avoid over-fitting. Atoms distant from the polymerase active site and the NNI-binding pocket (defined as atoms >20 Å from the Cα of Tyr-188) were tightly restrained to their rigid-body refined position, and strong stereochemical restraints were used. The progress of the refinement was monitored by cross-validation using 5% of the data. For example, the restrained isotropic B factor refinement for RTMC-1 reduced the R-free by 5.8%. Models were built into the electron density by using FRODO (22). Once cross-validation had established an optimum refinement strategy, the refinement was repeated by using all data to minimize over-fitting and to give a final model with an R-factor of 0.221 and very good stereochemistry (Table 1). For the lower-resolution datasets, only grouped B factor refinements were performed. Once more, the protocol was optimized by cross-validation against 5% of each dataset, but the actual refinement was performed using all data. A further check on the refinement was provided by the quality of the electron density of the inhibitor molecules, which were omitted from the phasing model.

The electron density map for RTMC-1 was of good quality, allowing confident identification of structural changes at both NNI and polymerase sites. The changes also were confirmed in the F_o-F_c maps calculated for RTMC-2 and RTMC-3. The F_o-F_c maps for the RTL74V structures clearly showed the leucine to valine substitution at residue 74 in the p51 subunit (Fig. 2*a*). To validate further the RTMC and L74V structures, we carried out intercrystal form electron density averaging by using the protocol described (6). This consisted of cyclic 3-fold cross averaging between equivalent domains in each crystal form but without internal averaging between domains within the heterodimer. The averaging procedure dramatically improved the electron density maps for the L74V structures, revealing small structural changes around residue 74 in the p51 subunit. Although the averaged density confirmed the reliability of the RTMC-1 structure, the averaged map was not improved significantly over the best of the individual maps, probably because of the large differences in the resolution of the three datasets.

All figures were produced by using BOBSCRIPT (23), a version of MOLSCRIPT (24) modified by R.M.E. and rendered with RASTER3D (25). RTMC-1 coordinates have been deposited at the Brookhaven Protein Data Bank.

RESULTS

Electron Density Maps for ddI-Resistant RTL74V. The electron density maps for the ddI-resistant RT show that there are no changes in the protein main chain of the p66 subunit associated with the side chain change of L74V. The density for the side chain of 74 is weak in both wild-type and ddI-resistant RT forms. This residue is exposed on the surface of the p66 subunit and is likely to become ordered fully only in the presence of template. By contrast, the side chain difference for this mutation is clear in the more buried environment of the p51 subunit, where negative electron density reflects the loss of a methylene group (Fig. 2*a*). Electron density averaging between the three crystal forms suggests that there are small main chain and side chain rear-

Table 1. Statistics for crystallographic structure determinations

RTMC data set	RTMC-1	RTMC-2	RTMC-3
Data collection details			
Data collection site	KEK BL-6A2	SRS 9.6	KEK BL-6A2
Wavelength (Å)	1.000	0.870	1.000
Collimation (mm)	0.10	0.18	0.10
Crystal form (no. of crystals)	F(1)	E(1)	C(3)
Unit cell dimensions (a, b, c in Å)	138.9, 114.4, 65.6	137.7, 109.8, 72.3	141.0, 110.4, 73.8
Resolution range (Å)	25.0–3.0	20.0–3.7	25.0–3.5
Observations	42,414	23,633	42,799
Unique reflections	17,935	10,424	13,658
Completeness (%)	83.3	85.9	89.9
Reflections with $F/\sigma(F) > 3$	13,580	8,328	10,334
R_{merge} (%)*	13.2	12.0	16.7
Outer resolution shell			
Resolution range (Å)	3.11–3.0	3.83–3.7	3.62–3.5
Unique reflections	1,375	945	1,122
Completeness (%)	64.2	79.4	79.9
Reflections with $F/\sigma(F) > 3$	581	629	518
R_{merge} (%)*	53.1	36.4	48.2
Refinement statistics			
Resolution range (Å)	25.0–3.0	8.0–3.8	8.0–3.5
No. of reflections	17,935	8,660	12,465
(working/test)	(17,038/897)	(8,227/433)	(11,842/623)
R-factor†	0.221	0.351	0.332
(R-work/R-free)	(0.264/0.335)	(0.352/0.378)	(0.332/0.347)
Protein atoms	7,577	7,842	7,891
Mean B-factor (Å^2)‡	48/56/44	30/34/−	39/45/−
rms backbone B-factor deviation	4.9	5.4	5.6
L74V data set	**RTL74V-1**	**RTL74V-2**	**RTL74V-3**
Data collection details			
Data collection site	KEK BL-6A2	KEK BL-6A2	SRS 7.2
Wavelength (Å)	1.000	0.940	1.488
Collimation (mm)	0.10	0.10	0.18
Crystal form (no. of crystals)	E(1)	C(2)	E(1)
Unit cell dimensions (a, b, c in Å)	136.9, 109.9, 73.5	139.6, 111.1, 73.5	136.7, 109.3, 71.2
Resolution range (Å)	25.0–3.4	25.0–3.2	25.0–3.3
Observations	45,234	38,412	40,907
Unique reflections	14,534	14,575	12,903
Completeness (%)	92.1	74.8	77.7
Reflections with $F/\sigma(F) > 3$	11,368	11,251	9,506
R_{merge} (%)*	12.5	12.1	12.1
Outer resolution shell			
Resolution range (Å)	3.52–3.4	3.31–3.2	3.42–3.3
Unique reflections	1,257	589	917
Completeness (%)	81.9	32.1	54.6
Reflections with $F/\sigma(F) > 3$	436	234	564
R_{merge} (%)*	50.0	51.4	35.7
Refinement statistics			
Resolution range (Å)	8.0–3.4	8.0–3.2	8.0–3.3
No. of reflections	13,472	13,571	11,824
(working/test)	(12,798/674)	(12,892/679)	(11,233/591)
R-factor†	0.357	0.331	0.331
(R-work/R-free)	(0.357/0.372)	(0.326/0.330)	(0.330/0.343)
Protein atoms	7,891	7,891	7,842
Mean B-factor (Å^2)‡	40/44/−	43/48/−	34/37/−
rms backbone B-factor deviation	5.0	5.3	5.4

The RTMC-1 structure was subjected to refinement with tight stereochemical restraints (rms deviation in bond lengths, 0.005 Å, and 1.2° in angles) whereas the others were refined by using only rigid-body and grouped B-factor refinements. In addition to the protein atoms given in the table, 22 inhibitor atoms were present in the RTMC-1 model. The structure determinations also benefited from intercrystal form electron density averaging for each mutant of RT (6).

*$R_{merge} = \Sigma|I - \langle I\rangle|/\Sigma\langle I\rangle$.

†R factor $= \Sigma|F_O - F_C|/\Sigma F_O$.

‡Mean B factor for main chain, side chain, and inhibitor atoms, respectively.

rangements of the nearby residues 72, 151, and 408–410 of the p51 subunit. This observation demonstrates that the methods and data are sufficient to allow us to detect very small changes within this relatively large (117 kDa) structure. We do not believe that these small changes in the p51 subunit can contribute to the ddI resistance of the L74V mutant because they are not propagated to the template or nucleotide triphosphate binding sites. Instead, from the position of this residue in the p66 subunit, close to the

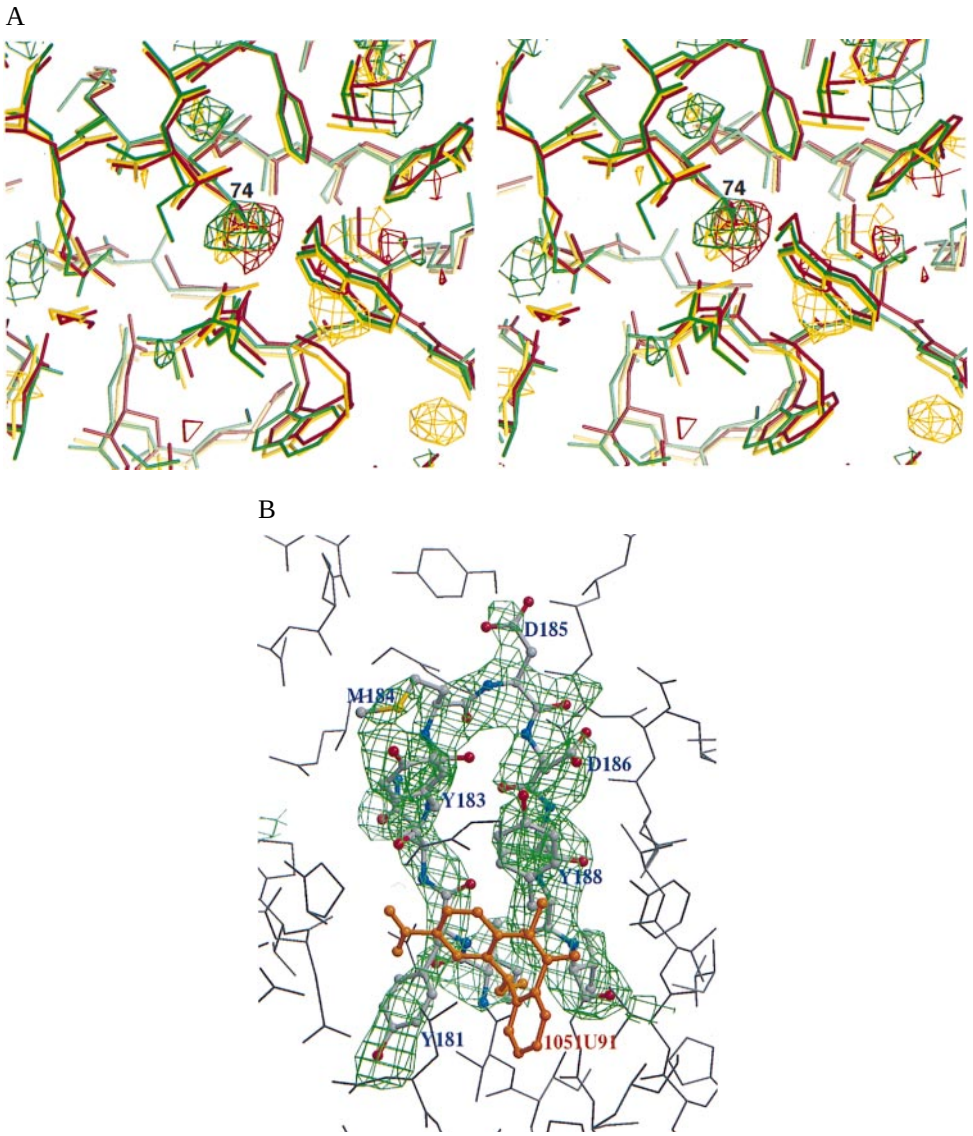

FIG. 2. Electron density maps. (*a*) A stereodiagram of Fo-Fc maps contoured at -2.5σ showing the negative electron density at residue 74 of the p51 subunit, indicating the Leu to Val substitution. The largest negative feature in the map was close to the inhibitor, which had been omitted from the model. The electron density and models for RTL74V-1, RTL74V-2, and RTL74V-3 are colored as red, yellow, and green, respectively. (*b*) An omit Fo-Fc map for the RTMC-1 data set contoured at 2.5σ showing the electron density for residues 180–189. The map was calculated from a model obtained by further refinement after removing these residues.

likely course of the incoming template strand, it seems plausible that the mutation affects drug selectivity indirectly via the bound template, as suggested (10).

Structure of AZT-Resistant RT (RTMC). Of the four amino acid changes of the AZT resistant RT (RTMC) relative to the HXB-2 wild type, D67N and K70R are in a similar region of the molecule to the L74V mutant and, in this case, no main chain movements could be detected in either p66 or p51. Indeed, within the p66 subunit, this region appeared flexible in both the wild-type and RTMC enzyme. This observation suggests that this part of the fingers domain may only become ordered on interaction with the template overhang. For these mutations, as for L74V, an indirect effect acting via the bound template seems plausible.

Of the remaining two mutations, at positions 215 and 219, the 215 mutation is pivotal, alone conferring 15- to 20-fold resistance (2). Structurally, the effect of these two mutations is quite different from that of changes at residues 67, 70, and 74; they cause a concerted movement of the structure, extending to the polymerase active site. Residues 215 and 219 lie within a loop leading to the β-sheet structure (β9, β10, and β11) that forms one half of a β-sandwich, which is completed by the β4, β7, and β8 sheet bearing the key active site residues. Inspection of difference maps, after initial refinement, revealed that this active site structure apparently was displaced in RTMC compared with its position in the wild-type enzyme. This observation was checked further by calculating a map in which residues 180 to 189 (contained within the β7 and β8 strands) were removed from the phasing model. The map clearly confirmed the new positions of these secondary structure elements (Fig. 2*b*). Overall, the maximum displacement is observed at β4 (1.2 Å in the vicinity of Asp-110), which is immediately adjacent to the loop containing the mutations at 215 and 219. At the more distal β8 strand, the displacement is somewhat less (1.0 Å at Asp-185). The exact mechanisms underlying this rearrangement are, however, unclear.

Changes in the NNI Site. The structural rearrangement seen in RTMC is propagated to the NNI binding site, leading to a reorientation of the side chain of Tyr-181, where a rotation of 160° occurs around the Cα–Cβ bond. This reorientation, in turn, results in a slight reorientation of the 1051U91 in the NNI pocket. The ring stacking interactions of the 1051U91 phenyl ring with Tyr-181 are replaced by less extensive contacts with the nitro

group; however, in compensation, there are more interactions with the side chain of Tyr-188. The ethyl group of 1051U91 is rotated by 145° from the orientation in the wild-type complex, leading to additional contacts with residues 188, 189, and 190 (Fig. 3*a*). Overall, there is an increase in the number of van der Waals contacts (<3.8 Å) between protein and inhibitor, presumably explaining the essentially unchanged IC_{50} for 1051U91 for RTMC when compared with the wild type (D.K.S, unpublished results). It has not proved possible to determine the structures of the unliganded forms of the mutant enzymes by our usual procedure of removing weakly bound inhibitors from preformed crystals (15). Despite this, we believe that the observed rearrangements of the RT active site seen in the NNI-inhibited enzyme could provide a mechanism capable of explaining the discrimination between the inhibitor, AZT-triphosphate, and the substrate, dTTP, achieved by this mutant enzyme.

Induced Movements in the RT Active Site. A movement of the three stranded β-sheet containing β4, β7 and β8 on binding of NNIs such as nevirapine to the unliganded enzyme has been reported (15), which provides a structural explanation of the mechanism of inhibition for this class of RT inhibitor. In the RTMC–NNI complex, the conformational change observed represents a further movement from the structure of the wild-type NNI-bound RT, having the effect of moving the active site residues back toward their position in the unliganded structure but not sufficiently to abolish NNI inhibition (Fig. 3*b*). This observation suggests that there is a preferred mode of conformational rearrangement around the RT active site that affects, with small movements, substrate discrimination whereas larger changes produce inhibition.

Reversal Effects of Tyr-181 on AZT Resistance. The change in the NNI site described above, particularly the rearrangement of Tyr-181, may have implications for the reported interactions between different sets of resistance mutations (26). Resistant viruses selected by NNIs commonly carry a mutation of residue 181 from tyrosine to cysteine (27). When this occurs in an AZT-resistant background such as RTMC, it has the effect of restoring AZT sensitivity (13, 28). The change that we see in the conformation of the Tyr-181 side chain may be relevant to this because the smaller Cys residue could cause the 215- and 219-induced rearrangement in the region of 181–188 to be attenuated, thus reversing the discriminatory effect and giving a resensitization to AZT. It is likely, however, that there are further mechanisms for such reversal effects because L74V also can restore

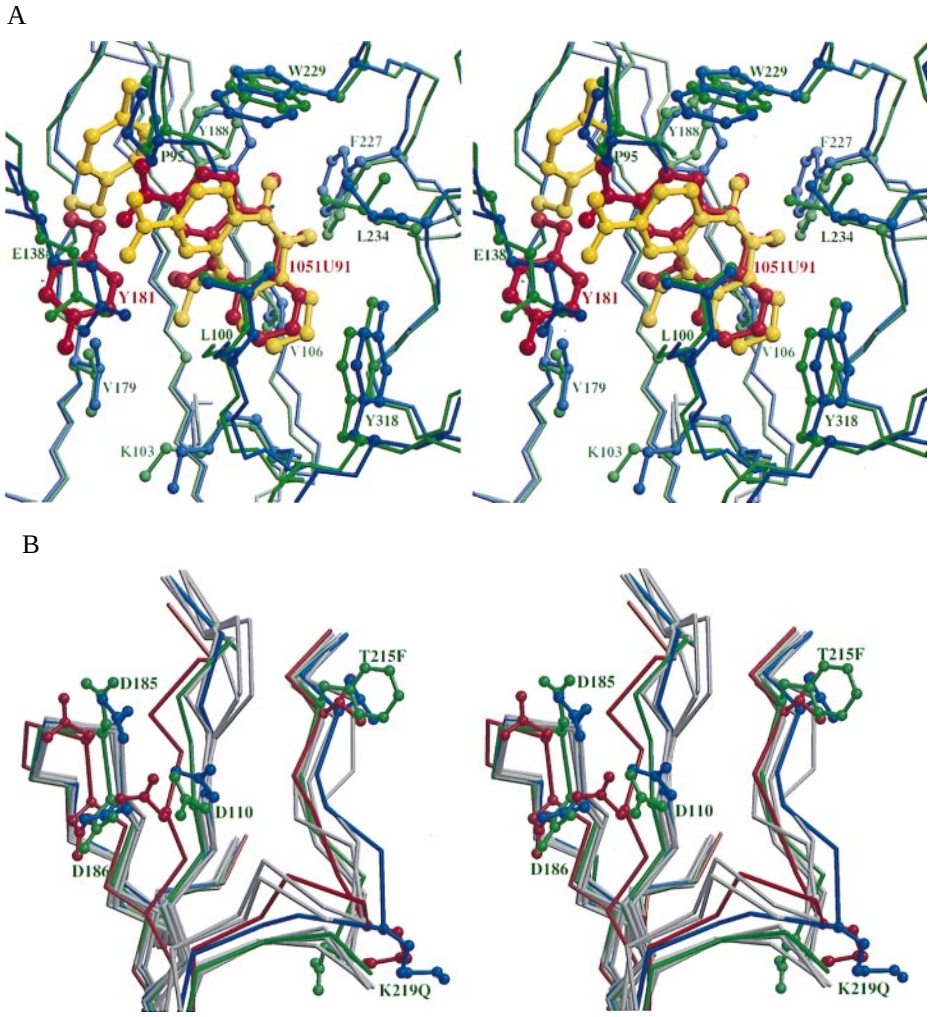

FIG. 3. The NNI binding site and polymerase active site. (*a*) A stereodiagram showing the superposition of the NNI binding site in RTMC and wild-type RT. The protein backbone is shown by thin sticks. The NNIs (thick bonds) and side chains that have contacts with the NNIs are shown as ball-and-stick representations. The RTMC is colored in green with residue 181 and the bound 1051U91 highlighted in red. The wild-type RT is colored in blue with residue 181 and bound 1051U91 highlighted in yellow. (*b*) A stereodiagram of the superposition of the active sites in RTMC (green), the wild type unliganded (red), and six NNI-bound RT structures (blue for RT-1051U91, gray for others) showing the structural changes at the active site in RTMC caused by 215 and 219 mutations. The Cα trace and side chains for residues 110, 185, 186, 215, and 219 are shown for RTMC, wild-type unliganded RT, and RT-1051U91; the Cα traces only are shown for RT-Cl-TIBO, RT-BHAP, RT-nevirapine, RT-MKC-442, and RT-α-APA. In the p51 subunit, residues 215 and 219 are disordered whereas residues 67 and 70 do not show significant rearrangement from the wild-type p51.

AZT sensitivity for certain resistance mutations (3), as can the 3′thiacytidine resistance mutation M184V (29).

DISCUSSION

This work indicates that there are likely to be at least two types of structural mechanism for drug resistance to NIs induced in RT by distal mutations. First, the mutations at 67, 70, and 74 do not give functionally significant conformational changes in the protein. Rather, they are in a position to derive their effect by altering the position of the DNA template. Second, one or both of the 215 and 219 mutations giving AZT resistance induce conformational changes in the RT active site. It is, therefore, not necessary to invoke a role for these particular mutations in an allosteric site on the p51 subunit (11) [which biochemical data also argue against (30)] nor in template rearrangement (10), particularly because our modeling studies suggest that these residues are unlikely to contact the template directly. Kinetic studies to assess the effect of the length of template overhang on the resistance of T215Y HIV-1 RT to AZT-triphosphate are not as yet available. Initial studies with HIV-2 RT containing the mutation S215Y (analogous to HIV-1 T215F), using 2′,3′-dideoxythymidine triphosphate as an inhibitor rather than AZT-triphosphate, showed no resistance effect even with a long template overhang (31). More recent work demonstrates essentially complete resistance irrespective of template length (32), consistent with our results.

Surprisingly, the structural changes induced by these AZT resistance mutations modulate the position of the active site amino acids with respect to the rest of the polymerase binding site in a mechanically similar way to that observed for transition from the NNI-bound to unliganded form. It seems that, even for a protein molecule such as HIV-1 RT, whose internal flexibility is well documented (6, 7, 33), the rigidity of the secondary structural components means that conformational changes at catalytic residues tend to occur in a characteristic way. This mechanistic linkage between two very different effects, NNI inactivation and modulation of substrate discrimination necessary for escape from an NI, may contribute to the success of treatment strategies that target the enzyme simultaneously with an NI and an NNI and help to explain the puzzling way in which escape from an NNI can resensitize a previously AZT-resistant virus.

We believe that a mutation at positions distant from the bound drug, giving rise to conformational changes to the binding site, represents a widely used mechanism for generation of drug resistance. In particular, such mechanisms are likely to provide a subtle method of introducing discrimination when the drug molecule mimics a substrate. Here, the scope for mutating contact residues is limited strictly because significant changes are likely to be incompatible with the maintenance of an active enzyme. Although to date, very few systems are characterized sufficiently well to test this hypothesis, it could explain the distal mutations resulting in sulfonamide resistance in dihydropteroate synthase (34) as well as those giving drug resistance in HIV protease (35). The more general importance of distal mutations in modulating the affinity of ligand binding is reinforced by the recent report (36) that mutations up to 15 Å from the antigen binding-site contribute to the affinity maturation for an antibody.

We thank the staffs of the Synchrotron Radiation Source, Daresbury Laboratory, United Kingdom and the Photon Factory, National Laboratory for High Energy Physics, Japan for their help with data collection; Richard Bryan and Kathryn Measures for computing support and Steven Lee for photographic support. The Oxford Centre for Molecular Sciences is supported by the Biotechnology and Biological Sciences Research Council, the Medical Research Council, and the Engineering and Physical Sciences Research Council. E.Y.J. is supported by the Royal Society; D.I.S. and D.K.S. are supported by the Medical Research Council. The AIDS-directed program of the Medical Research Council has provided long-term funding for this project, with grants to D.I.S. and D.K.S.

1. Balter, M. (1996) *Science* **274,** 1988–1989.
2. Larder, B. A. & Kemp, S. D. (1989) *Science* **246,** 1155–1158.
3. St. Clair, M. H., Martin, J. L., Tudor-Williams, G., Bach, M. C., Vavro, C. L., King, D. M., Kellam, P., Kemp, S. D. & Larder, B. A. (1991) *Science* **253,** 1557–1559.
4. Kohlstaedt, L. A., Wang, J., Friedman, J. M., Rice, P. A. & Steitz, T. A. (1992) *Science* **256,** 1783–1790.
5. Jacobo-Molina, A., Ding, J. P., Nanni, R. G., Clark, A. D. J., Lu, X., Tantillo, C., Williams, R. L., Kamer, G., Ferris, A. L., Clark, P., *et al.* (1993) *Proc. Natl. Acad. Sci. USA* **90,** 6320–6324.
6. Ren, J., Esnouf, R., Garman, E., Somers, D., Ross, C., Kirby, I., Keeling, J., Darby, G., Jones, Y., Stuart, D. *et al.* (1995) *Nat. Struct. Biol.* **2,** 293–302.
7. Rodgers, D. W., Gamblin, S. J., Harris, B. A., Ray, S., Culp, J. S., Hellmig, B., Woolf, D. J., Debouck, C. & Harrison, S. C. (1995) *Proc. Natl. Acad. Sci. USA* **92,** 1222–1226.
8. Smerdon, S. J., Jager, J., Wang, J., Kohlstaedt, L. A., Chirino, A. J., Friedman, J. M., Rice, P. A. & Steitz, T. A. (1994) *Proc. Natl. Acad. Sci. USA* **91,** 3911–3915.
9. Ding, J., Das, K., Tantillo, C., Zhang, W., Clark, A. D. J., Jessen, S., Lu, X., Hsiou, Y., Jacobo-Molina, A., Andries, K, *et al.* (1995) *Structure* **3,** 365–379.
10. Boyer, P. L., Tantillo, C., Jacobo-Molina, A., Nanni, R. G., Ding, J., Arnold, E. & Hughes, S. H. (1994) *Proc. Natl. Acad. Sci. USA* **91,** 4882–4886.
11. Yadav, P. N. S., Yadav, J. S. & Modak, M. J. (1995) *Nat. Struct. Biol.* **2,** 193–195.
12. Stammers, D. K., Somers, D. O. N., Ross, C. K., Kirby, I., Ray, P. H., Wilson, J. E., Norman, M., Ren, J., Esnouf, R. M., Garman, E. F. *et al.* (1994) *J. Mol. Biol.* **242,** 586–588.
13. Larder, B., Purifoy, D., Powell, K. & Darby, G. (1987) *EMBO J.* **6,** 3133–3137.
14. Hargrave, K. D., Proudfoot, J. R., Grozinger, K. G., Cullen, E., Kapadia, S. R., Patel, U. R., Fuchs, V. U., Mauldin, S. C., Vitous, J., Behnke, M. L., *et al.* (1991) *J. Med. Chem.* **34,** 2231–2241.
15. Esnouf, R., Ren, J., Ross, C., Jones, Y., Stammers, D. & Stuart, D. (1995) *Nat. Struct. Biol.* **2,** 303–308.
16. Ren, J., Esnouf, R., Hopkins, A., Ross, C., Jones, Y., Stammers, D. & Stuart, D. (1995) *Structure* **3,** 915–926.
17. Sakabe, N. (1991) *Nucl. Instr. Methods Phys. Res.* **303,** 448–463.
18. Otwinowski, Z. (1993) in *Data Collection and Processing*, eds. Sawyer, L., Isaacs, N. & Bailey, S. (SERC Daresbury Laboratory, Warrington, U.K.), pp. 56–62.
19. Brunger, A. T. (1992) X-PLOR *Manual* (Yale Univ. Press, New Haven, CT).
20. Hopkins, A. L., Ren, J., Esnouf, R. M., Willcox, B. E., Jones, E. Y., Ross, C., Miyasaka, T., Walker, R. T., Tanaka, H., Stammers, D. K. *et al.* (1996) *J. Med. Chem.* **39,** 1589–1600.
21. Esnouf, R. M., Ren, J., Hopkins, A. L., Ross, C. K., Jones, E. Y., Stammers, D. K. & Stuart, D. I. (1997) *Proc. Natl. Acad. Sci. USA* **94,** 3984–3989.
22. Jones, T. A. (1985) *Methods Enzymol.* **115,** 157–171.
23. Esnouf, R. M. (1997) *J. Mol. Graphics* **15,** 133–138.
24. Kraulis, P. J. (1991) *J. Appl. Crystallogr.* **24,** 946–950.
25. Merritt, E. A. & Murphy, M. E. P. (1994) *Acta Crystallogr. D* **50,** 869–873.
26. Larder, B. A. (1994) *J. Gen. Virol.* **75,** 951–957.
27. De Clercq, E. (1994) *Biochem. Pharmacol.* **47,** 155–169.
28. Larder, B. A. (1992) *Antimicrob. Agents Chemother.* **36,** 2664–2669.
29. Larder, B. A., Kemp, S. D. & Harrigan, P. R. (1995) *Science* **269,** 696–699.
30. Boyer, P. L. & Hughes, S. H. (1996) *Nat. Struct. Biol.* **3,** 579–580.
31. Perach, M., Rubinek, T. & Hizi, A. (1995) *J. Virol.* **69,** 509–512.
32. Perach, M., Rubinek, T., Hughes, S. H. & Hizi, A. (1997) *J. Mol. Biol.* **268,** 648–654.
33. Jager, J., Smerdon, S. J., Wang, J., Boisvert, D. C. & Steitz, T. A. (1994) *Structure* **2,** 869–876.
34. Hampele, I. C., D'Arcy, A., Dale, G. E., Kostrewa, D., Nielsen, J., Oefner, C., Page, M. G. P., Schonfeld, H.-J., Stuber, D. & Then, R. L. (1997) *J. Mol. Biol.* **268,** 21–30.
35. Erickson, J. W. & Burt, S. K. (1996) *Annu. Rev. Pharmacol. Toxicol.* **36,** 545–571.
36. Wedemayer, G. J., Patten, P. A., Wang, L. H., Schultz, P. G. & Stevens, R. C. (1997) *Science* **276,** 1665–1669.
37. Kellam, P., Boucher, C. A., Tijnagel, J. M. & Larder, B. A. (1994) *J. Gen. Virol.* **75**, 341–351.